nature nanotechnology

LETTERS

PUBLISHED ONLINE: 20 DECEMBER 2009 | DOI: 10.1038/NNANO.2009.452

Colloidal lenses allow high-temperature single-molecule imaging and improve fluorophore photostability

Jerrod J. Schwartz†, Stavros Stavrakis† and Stephen R. Quake*

Although single-molecule fluorescence spectroscopy was first demonstrated at near-absolute zero temperatures (1.8 K)[1], the field has since advanced to include room-temperature observations[2], largely owing to the use of objective lenses with high numerical aperture, brighter fluorophores and more sensitive detectors. This has opened the door for many chemical and biological systems to be studied at native temperatures at the single-molecule level both *in vitro*[3–4] and *in vivo*[5–6]. However, it is difficult to study systems and phenomena at temperatures above 37 °C, because the index-matching fluids used with high-numerical-aperture objective lenses can conduct heat from the sample to the lens, and sustained exposure to high temperatures can cause the lens to fail. Here, we report that TiO_2 colloids with diameters of 2 μm and a high refractive index can act as lenses that are capable of single-molecule imaging at 70 °C when placed in immediate proximity to an emitting molecule. The optical system is completed by a low-numerical-aperture optic that can have a long working distance and an air interface, which allows the sample to be independently heated. Colloidal lenses were used for parallel imaging of surface-immobilized single fluorophores and for real-time single-molecule measurements of mesophilic and thermophilic enzymes at 70 °C. Fluorophores in close proximity to TiO_2 also showed a 40% increase in photostability due to a reduction of the excited-state lifetime.

Integrated optical elements such as colloidal lenses have been used to focus or collect light in a variety of applications. For example, hemispherical solid immersion lenses[7] and spherical colloidal lenses have been used to construct a rotational sensor[8,9], to create an optomagnetic dimmer[10], to manipulate a light beam[11], to generate two-dimensional micropatterns and nanopatterns[12–14] and to optically couple one-dimensional arrays of colloidal particles[15]. Wenger and colleagues[16] recently demonstrated that a latex microsphere in conjunction with a low numerical-aperture (NA) objective lens can be used for fluorescence-correlation spectroscopy with near single-molecule sensitivity. An efficient nanolens system based on gold nanosphere aggregates was shown to have a strong electromagnetic surface-enhanced Raman scattering (SERS) enhancement, demonstrating the potential of nanolenses for single-molecule SERS[17]. However, these techniques have not yet achieved true single-molecule sensitivity. Single-molecule detection in droplets[18] and flowing sample streams[19] has been demonstrated with long working distance and low-NA optics, but these approaches do not combine parallelization with the observation of time traces and have not been demonstrated at high temperatures. In one non-fluorescent single-molecule study, the temperature dependence of rotation and hydrolysis of the F1-ATPase was monitored by attaching a polystyrene bead to the rotor subunit. The rotation rate of the motor was inferred by observing the bead motion in conditions ranging from 4 to 50 °C (ref. 20).

Geometric optics can be used to estimate the collection efficiency of a micrometre-sized colloidal lens. The configuration is illustrated in Fig. 1a and has been previously described for the lensing of a smaller fluorescent microsphere[8]. By selecting spherical colloids composed of a high-index refraction material such as TiO_2 ($n_2 \geq 2.0$), the absolute value of the exit angle in water ($n_1 = 1.33$) is always less than 25°, even for very large angles of incidence (Fig. 1b). If θ_0 is the semi-aperture of an external microscope objective, any exit ray with $\phi' - \theta'' < \theta_0$ will be collected. TiO_2 colloidal lenses should therefore improve the effective NA of a low-NA air objective (0.5 NA, $\theta_0 = 30°$) to $NA_{eff} = (2.0)\sin(84°) = 1.99$. Higher values of θ will probably cause the light to undergo total internal reflection (TIR) within the colloid.

Finite-difference time-domain (FDTD) simulations were performed with the Meep software package (see Supplementary Information) to more rigorously determine how key parameters of the system affect the collection efficiency[21]. A point source was positioned next to a spherical colloid and the power P transmitted through a plane on the opposite side of the lens was calculated (Fig. 1c). The power was normalized by dividing it by the total power emitted by the point source in all directions without the colloid present. Different plane dimensions were chosen to represent the semi-aperture light collection of 14 different microscope objectives ($1° \leq \theta_0 \leq 65°$). The relationship between the index n_2 of the colloid and P is shown in Fig. 1d, where high-index colloids are shown to provide the greatest relative enhancement for objectives with small semi-apertures. For example, the collection efficiency of an $n_2 = 2.4$ colloidal lens-aided 0.3 NA air objective was improved nearly eightfold compared to that obtained using the objective alone. Even high-NA objectives had a modest approximately twofold improvement with the use of $n_2 = 1.6$–1.8 colloids. Simulations were also run to determine how P is influenced by changing the distance between the fluorophore and the colloid, the radius of the colloid, and the wavelength of the emitted light (Supplementary Fig. S1).

The simulations predict that $n_2 = 2.0$ colloids should allow a 0.5 NA air objective ($\theta_0 = 30°$) to achieve a 44% improvement in light collection efficiency compared to a 1.4 NA oil-immersion objective ($\theta_0 = 67°$). The simulations therefore predict an effective NA of 1.68, which is slightly lower than the 1.99 effective NA predicted by ray optics. We first tested this by imaging individual quantum dot nanoparticles and found that 2.0 μm TiO_2 colloidal lenses had an effective NA of ~1.44. This substantially exceeds the performance of conventional air-gap objectives and matches all but the most exotic oil-immersion objectives in use today.

Department of Bioengineering, Stanford University and Howard Hughes Medical Institute, Stanford, California 94305, USA; †These authors contributed equally to this work. *e-mail: quake@stanford.edu

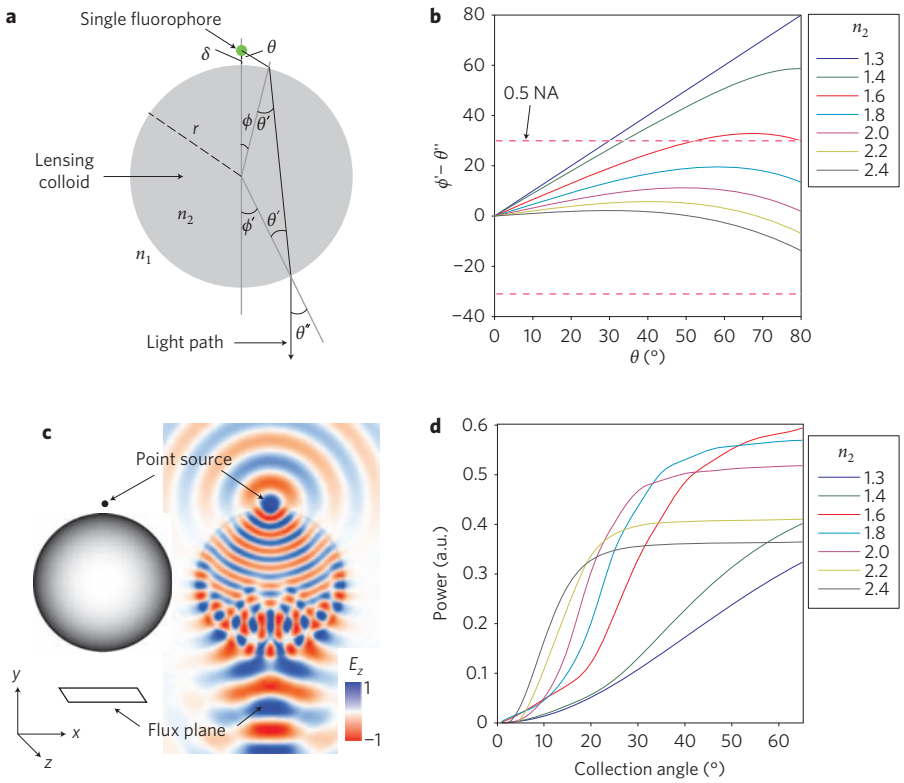

Figure 1 | Spherical colloids are efficient lenses for single-molecule imaging. a, Light-ray tracing of photons emitted from a nearby single fluorophore undergoing lensing through a colloid. The diagram defines the angles θ, θ', θ'', ϕ and ϕ' and the distances r and δ as previously described[8]. **b**, Plot showing the ray exit angle ($\phi' - \theta''$) versus the emission angle from the fluorophore (θ) for $n_2 = 1.33$–2.40. The dashed horizontal lines define the ray collection limits for a 0.5 NA objective. **c**, The left panel shows the geometric model used for the FDTD simulations; the right shows the results of the simulations. A point source ($\lambda_o = 570$ nm) was placed $\delta = 0.010$ μm ($y = 0.010$) away from a 2.0 μm spherical dielectric ($n_2 = 2.0$) in an aqueous environment ($n_1 = 1.33$). The E_z field intensity in arbitrary units is shown in blue/red along the $z = 0$ plane. **d**, Normalized power through the flux plane calculated as a function of the flux plane dimensions, which was then converted into an effective objective semi-aperture. The refractive index of the lens was varied from $n_2 = 1.33$ to 2.40.

However, the efficiency is slightly lower than the simulations predict, and the discrepancy might be explained by less than perfect transmission of the colloid or some variation of the surface interactions described below. Scanning electron microscopy (SEM) images of the TiO_2 colloids confirmed that they were spherical in shape (Supplementary Fig. S2).

Biotinylated 2.0 μm TiO_2 colloids were then coupled to a surface containing single molecules of Cy3-labelled streptavidin (Fig. 2a). The surface was dried, inverted and imaged using epifluorescent excitation with light collection through a ×20 0.5 NA air objective. Signals were only detected where colloids were immobilized, and each signal showed a stepwise decrease to background, which was indicative of the presence of a single fluorophore (Fig. 2c,d). The surface was heated from 23 °C to 70 °C and single-step photobleaching was still observed, even at high temperature (Fig. 2e). In the absence of colloids, no signal was detected with a ×20 0.5 NA objective.

We observed single molecules in aqueous samples with colloidal lenses by changing the excitation geometry from epifluorescence to prism-based total internal reflection (TIR) excitation (Fig. 2b). Cy3-labelled dsDNA was coupled to TiO_2 colloids and allowed to bind to an aminated glass surface. At 23 °C, ~30% of the colloids emitted fluorescence, and each signal showed stepwise photobleaching (Fig. 2f). Signals were only detected where colloids were immobilized and not in the area between the colloids. The 70% of the colloids that did not fluoresce were either not coupled to a fluorophore or the fluorophore was not correctly aligned for lensing. Stepwise photobleaching was also observed at 70 °C after taking precautions to minimize evaporation in a custom-made high-temperature flow cell (Fig. 2g).

Bleaching times from over 100 molecules were analysed from each of these experiments (Fig. 2h–k). An approximately twofold reduction in lifetime was observed in going from 23 °C to 70 °C for both the dry and wet samples, which might be explained by an increase in the reaction rates of molecules in excited or triplet states with singlet molecular oxygen. The photon flux at the camera for the colloidal lenses with a ×20 0.5 NA objective was $\sim 0.8 \times 10^4$ photons s^{-1} in air with epifluorescence excitation and $\sim 0.6 \times 10^4$ photons s^{-1} in water with prism TIR excitation. This is less than that of a ×60 1.40 NA objective in the absence of colloidal lenses ($\sim 2.2 \times 10^4$ photons s^{-1}), due largely to photophysical interactions of the fluorophore with the colloid.

We measured fluorescent intensities and lifetimes in an optical configuration in which the laser excitation and detected fluorophore emission did not propagate through the colloid in order to characterize the photophysical effect of the colloid (Fig. 3a–c). Single molecules of Cy3–streptavidin were bound to a cover slip and imaged using through the objective TIR and a high-NA objective (NA 1.45, ×60) with and without TiO_2 colloids. The average detected photon flux decreased 40% in the presence of the TiO_2 colloid. Lifetimes were similar in the absence of a colloid (Fig. 3a) or in the presence of a polystyrene colloid (Fig. 3b), but the mean photobleaching lifetime increased by 40% with TiO_2 colloids present (Fig. 3c). Taken together, this suggests that the TiO_2 colloids cause quenching to take place either through resonance energy transfer or electron transfer from the excited fluorescent molecule to the conduction band of TiO_2. Quenching also explains the higher photostability, because molecules spend less time in the

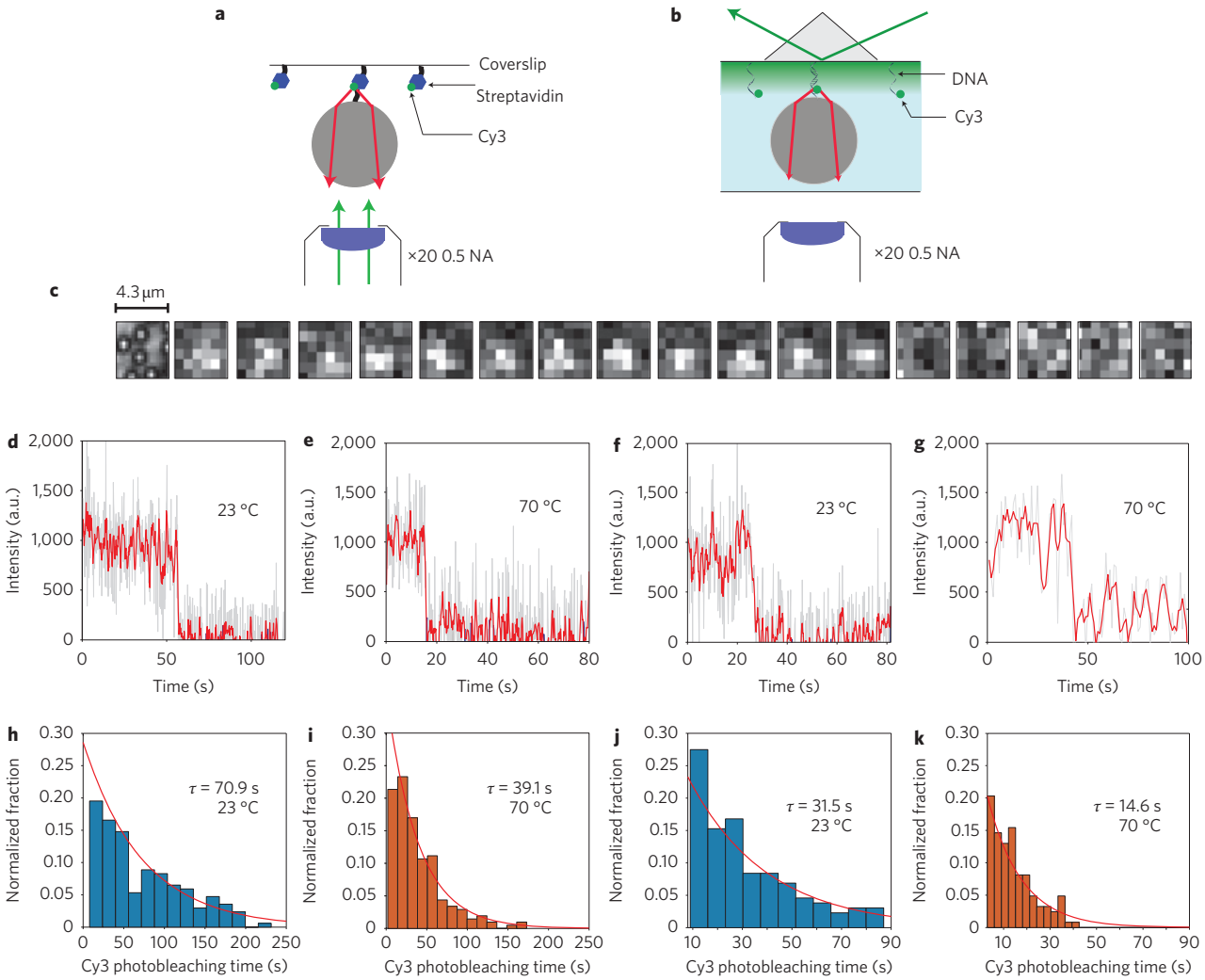

Figure 2 | Single fluorophores in dry and wet samples can be imaged efficiently with colloidal lenses and a low light collection efficiency objective. **a**, Schematic of the epifluorescent optical configuration for dry samples. TiO_2 colloids (2.0 µm) were biotinylated and coupled to surface-immobilized Cy3–streptavidin. Excitation and light collection was achieved with a ×20 0.5 NA air objective. **b**, Schematic of the prism TIR optical setup for wet samples. TiO_2 colloids (2.0 µm) were functionalized with Cy3-labelled DNA and immobilized on a surface in an aqueous environment. Excitation was achieved by means of prism TIR and light collection with a ×20 0.5 NA air objective. **c**, The first image in this series is a bright-field image showing the relative spatial position and size of a 2.0 µm TiO_2 colloid coupled to a surface through Cy3–streptavidin. The remaining images are taken with a different camera and depict the epifluorescent excitation and emission at the same spatial position at intervals of 0.5 s. Single-step photobleaching was observed at 23 °C (**d**) and at 70 °C (**e**). With a tether of Cy3-labelled dsDNA and prism TIR excitation, stepwise photobleaching was also observed at 23 °C (**f**) and 70 °C (**g**) (raw time traces are shown in grey and three-point smoothing traces in red). Photobleaching lifetimes of Cy3 varied for dry (**h**,**i**) and wet (**j**,**k**) samples and decreased with an increase in temperature.

exited state and are able to undergo more excitation–emission cycles before photobleaching. The use of an oxygen scavenging system did not significantly affect the mean photobleaching lifetime of Cy3 when it was coupled to TiO_2, also possibly due to molecules spending less time in the excited state.

Energy transfer from an excited molecule to a semiconductor surface has been shown to have a d^{-3} distance dependence on the fluorescence lifetime for 10 nm $< d <$ 43 nm (refs 22,23), a regime that includes the distances used in the present study. This quenching mechanism has also been reported for metal surfaces[24]. For TiO_2, a decrease in fluorescence lifetime due to quenching has been reported for cresyl violet over 10 nm $< d <$ 50 nm but the mechanism of non-radiative energy transfer was not identified[25]. The exact mechanism for this non-radiative decay process near semiconductors is not clear and requires further study, and it is possible that more careful control of the distance between the colloid and the fluorophore can be used to optimize the balance between lensing enhancement and quenching effects. Photoluminescence is known to increase for quantum dots near metallic nanostructures[26], but does not significantly change for quantum dots on TiO_2 nanocrystalline thin films[27]. Relative differences in the electron transfer rates from either quantum dots[27,28] or organic fluorophores[29] to TiO_2 might explain the observed variation in quenching and collection efficiency.

We used colloidal lenses to measure real-time single-molecule kinetics of a thermophilic DNA polymerase at 70 °C (Therminator from *Thermococcus 9°N*). Details of the assay have been described for a study of mesophilic DNA polymerase kinetics[30] (Fig. 4a). The DNA template contains an internal double-stranded 33 bp hairpin; the 3′ base of the hairpin contains an internal Cy3 Förster resonance energy transfer (FRET) donor and the 5′ base contains an internal non-fluorescent FRET acceptor, so that when the hairpin is fully folded, quenching of Cy3 by BHQ-2 prevents any fluorescence emission. Both ends of the template were functionalized to allow for attachment to the surface and the colloid. On the addition of a

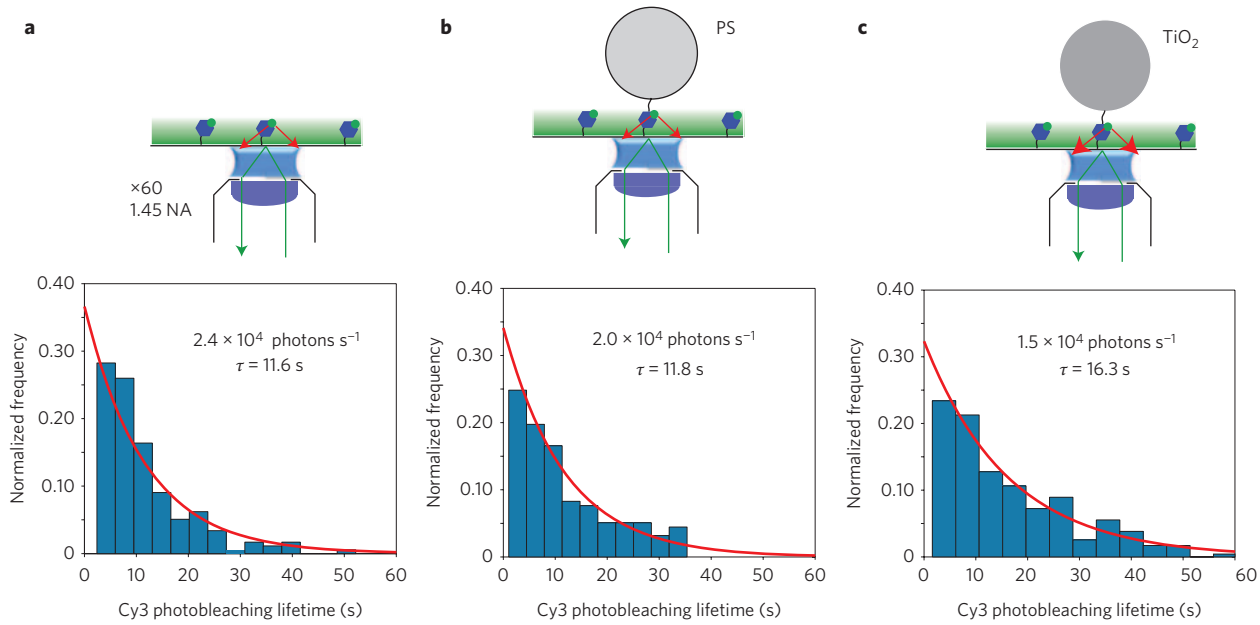

Figure 3 | Cy3 photobleaching lifetimes increase in the presence of TiO_2 colloids. a, In the absence of colloids and colloidal lensing, Cy3-labelled streptavidin had a mean lifetime of 11.6 s under TIR excitation with a ×60 1.45 NA objective (excitation intensity 3.3 mW) . **b**, The mean photobleaching lifetime with polystyrene colloids (PS) stayed nearly the same at 11.8 s. **c**, In the presence of TiO_2 colloids, the lifetime increased to 16.3 s.

DNA polymerase with strand displacement activity and all four deoxynucleotide triphosphates (dNTPs), the primer is extended through the hairpin to recover Cy3 fluorescence.

Control experiments taken with a ×60 1.45 NA oil objective without colloidal lenses showed fast replication without pausing (Fig. 4b), fast replication with a single pause at a motif known to induce pausing (Fig. 4c), and stepwise refolding of the hairpin after replication (Fig. 4d), in agreement with previous studies[30]. We first verified that the addition of the TiO_2 colloid to the distal end of the template did not prevent polymerase activity by performing the experiments at room temperature with the Klenow fragment of DNA polymerase I from *Escherichia coli*. On addition of the extension mixture to hairpins coupled to colloidal lenses at 23 °C, replication through the hairpin was detected with a ×20 0.5 NA air objective as a decrease in FRET efficiency and recovery of Cy3 signal. As with the ×60 1.45 NA objective, single-molecule trajectories with the colloidal lenses showed fast replication (Fig. 4e), fast replication with a single pause (Fig. 4f)[30], fast replication with multiple pauses, and stepwise refolding of the hairpin after replication (Fig. 4g). The fact that colloidal lenses detected strand displacement synthesis and heterogeneous pausing similar to that observed with a 1.45 NA objective illustrates the sensitivity and capability of this approach for biological assays. The pause efficiency was slightly reduced (25 to 10%) with the colloid present, but the duration of pauses increased twofold (from 13 to 25 s; Supplementary Fig. S5a and ref. 30); this may be due to increased template tension induced by thermal fluctuations of the colloid. If Pol I(KF) or the dNTPs were omitted from the extension mixture or if the colloids were not coupled to the hairpin, there was no significant recovery of Cy3 signal.

To measure the real-time single-molecule kinetics of Therminator DNA polymerase, some details of the assay were modified to accommodate higher operating temperature (see Supplementary Information). Single-molecule trajectories of Therminator activity at 70 °C measured with colloidal lenses and a ×20 0.5 NA air objective showed fast replication (Fig. 4h), fast replication with a single pause (Fig. 4i), fast replication with multiple pauses, and stepwise refolding of the hairpin after replication (Fig. 4j). The frequency of pausing during Therminator replication at 70 °C was reduced from 10 to 5% of all trajectories compared to Pol I(KF) at 23 °C, and the frequency of stepwise refolding was also reduced from 13 to 5%. Incorporation rates for Pol I(KF) and Therminator were measured by first generating a calibration curve between Cy3 intensity and DNA polymerase position based on the location of the known pause motif. The intensities along each trajectory were then converted into positions and the rates were calculated by measuring the slope of the trajectory between two steady states. The measured rate of 12 nucleotides per second (nt s^{-1}) for Pol I(KF) (Fig. 4k) was slightly slower than measured in the absence of the colloid with a ×60 1.45 NA objective (14 nt s^{-1})[30], possibly because the replicating polymerase follows the helical backbone resulting in colloid rotation. The measured rate for Therminator of 13 nt s^{-1} at 70 °C (Fig. 4l) is triple the vendor's reported polymerase chain reaction (PCR) rate of 4 nt s^{-1}, suggesting that the pausing behaviour we distinguish with our single-molecule experiments may be included in ensemble studies (Supplementary Fig. S5b). The separation of burst synthesis from sequence-specific pausing can only be realized in a single-molecule experiment.

The ability of colloidal lenses to image very large fields of view at high temperatures with single-molecule sensitivity, free of the restraints of index-matching fluids and short working distances, could improve the sensitivity of hand-held microscopes and biological detectors and also have applications in other areas of biology and chemistry. For example, single-molecule sequencing-by-synthesis technologies currently use a mesophilic DNA polymerase to sequentially incorporate fluorescently labelled nucleotides into a growing complementary strand. The ability to use a thermophilic polymerase would offer improved enzyme heat stability, better ability to incorporate nucleotide analogues, and the capacity to melt templates that are GC-rich or have a high degree of secondary structure. The throughput of single-molecule DNA sequencing methods is also limited by the number of templates visible in a single field of view[31]; integrating colloidal lenses directly into the imaging hardware could increase throughput by an order of magnitude.

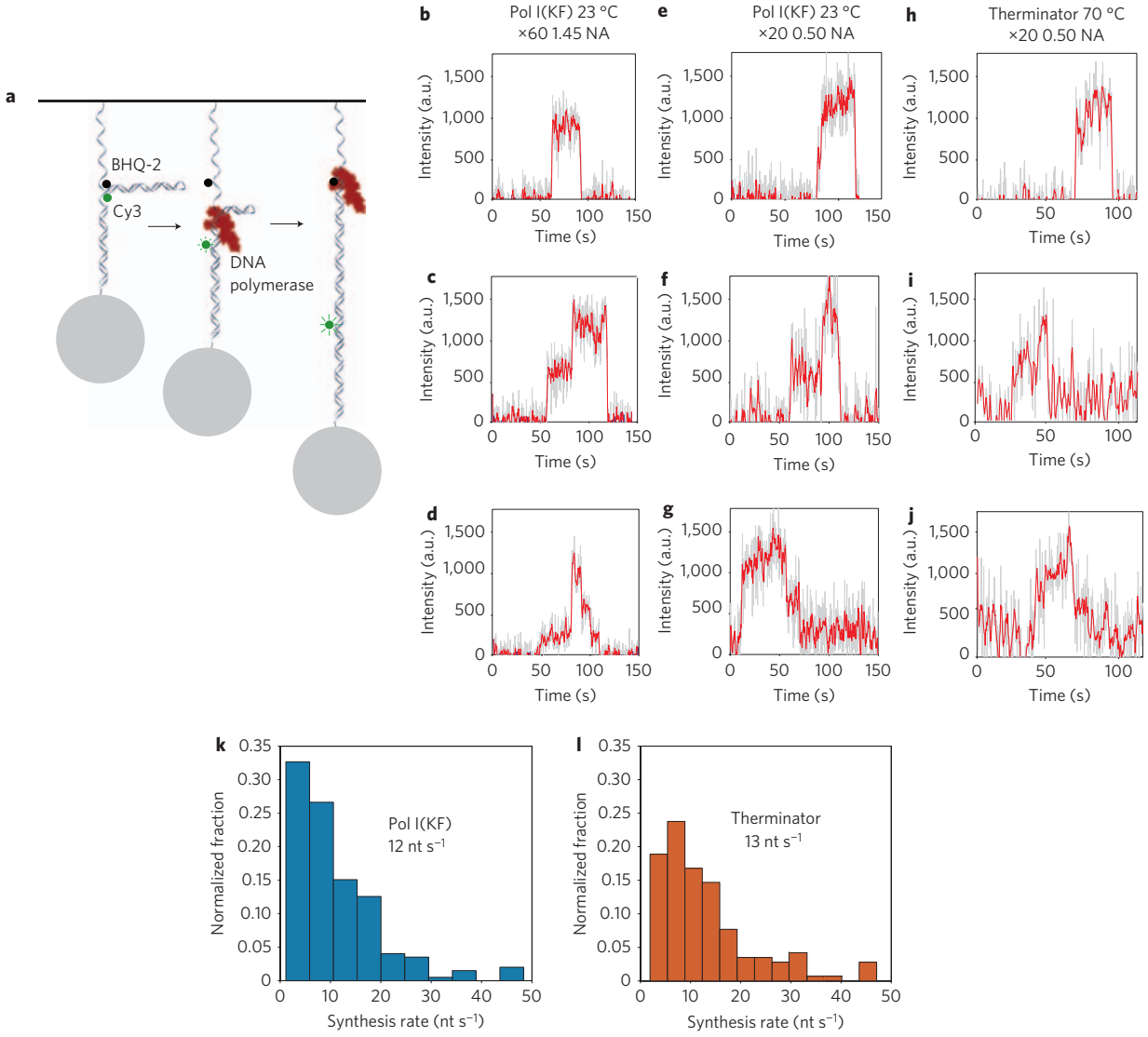

Figure 4 | Single-molecule DNA polymerase activity can be observed with colloidal lenses and a ×20 0.5 NA air objective. a, Schematic of the DNA template used to measure real-time polymerase kinetics. Primed 259 nt DNA molecules containing internal 33 bp hairpins and flanking 94 nt tails were immobilized on a glass surface through a biotin–streptavidin linker. DNA replication through the hairpin resulted in a reduction in FRET efficiency between Cy3 and BHQ-2, giving rise to an increase in Cy3 fluorescence. **b–d**, Trajectories of this process imaged with a ×60 1.45 NA oil-immersion objective without colloidal lenses show different behaviours, including fast extension (**b**), pausing during fast extension (**c**) and refolding of the hairpin into a cruciform structure (**d**). **e–j**, Trajectories exhibiting similar behaviours were observed with a ×20 0.5 NA air objective with colloidal lenses. **k–l**, Histograms of the measured replication rates for Pol I(KF) (**k**) and Therminator DNA (**l**) polymerases.

Methods

Carboxylated and aminated TiO_2 colloids (Corpuscular Inc.) and RCA clean glass cover slips (Precision Glass & Optics) were functionalized with standard bioconjugation techniques. Typically biotin–neutravidin or digoxigenin/anti-digoxigenin binding were used for non-covalent coupling and polyethylenimine and diisothiocyanate (DITC) were used for covalent bonding. Functionalized quantum dots (Invitrogen) and DNA oligonucleotides (Integrated DNA Technologies and Operon) were coupled to the reactive colloids using empirically determined concentrations. DNA templates containing an internal hairpin were constructed by ligating four separate synthetic oligonucleotides together with Ampligase (Epicenter Technologies). For the kinetics experiments, TiO_2 colloids were functionalized with ssDNA and hybridized to surface-bound templates or were decorated with dsDNA and bound directly to a reactive surface. A buffered mixture containing 200−300 μM dNTPs and 10 units of DNA polymerase (Klenow exo- or Therminator, New England Biolabs) was added to the flow cell to start the reaction. Images were acquired with prism TIR excitation using a ×20 0.5 NA objective and custom software written in LabVIEW (National Instruments). For the high-temperature experiments, the cover slip was placed in a modified flow cell containing a circular resistor heater. The optical setup for epifluorescence, prism TIR and through the objective TIR imaging was based around a Nikon TE-2000S inverted microscope equipped with either a Nikon Plan Fluor ×20 0.5 NA air objective, a Nikon PlanApo ×60 1.45 NA TIRF oil objective, or a Nikon ×60 1.4 NA oil objective. Samples were illuminated using a 50 W mercury lamp or a diode-pumped 532 nm laser (CrystaLaser) with appropriate excitation and emission filters (Chroma). *XY* motion was controlled with a motorized stage (Mad City Labs), focus control was manually set with a Z-drive controller (ASI Scientific), and images were acquired on an electron-multiplying charge-coupled device (EM-CCD) camera (Cascade II 512).

Received 1 September 2009; accepted 16 November 2009; published online 20 December 2009

References

1. Orrit, M. & Bernard, J. Single pentacene molecules detected by fluorescence excitation in a p-terphenyl crystal. *Phys. Rev. Lett.* **65,** 2716–2719 (1990).
2. Betzig, E. & Chichester, R. J. Single molecules observed by near-field scanning optical microscopy. *Science* **262,** 1422–1425 (1993).
3. Ambrose, W. P. *et al.* Single molecule fluorescence spectroscopy at ambient temperature. *Chem. Rev.* **99,** 2929–2956 (1999).

4. Weiss, S. Fluorescence spectroscopy of single biomolecules. *Science* **283,** 1676–1683 (1999).
5. Yu, J., Xiao, J., Ren, X., Lao, K. & Xie, X. S. Probing gene expression in live cells, one protein molecule at a time. *Science* **311,** 1600–1603 (2006).
6. Sako, Y., Minoghchi, S. & Yanagida, T. Single-molecule imaging of EGFR signalling on the surface of living cells. *Nature Cell. Biol.* **2,** 168–172 (2000).
7. Koyama, K., Yoshita, M., Baba, M., Suemoto, T. & Akiyama, H. High collection efficiency in fluorescence microscopy with a solid immersion lens. *Appl. Phys. Lett.* **75,** 1667–1669 (1999).
8. Brody, J. P. & Quake, S. R. A self-assembled microlensing rotational probe. *Appl. Phys. Lett.* **74,** 144–146 (1999).
9. Helseth, L. E. & Fischer, T. M. Cooperative microlenses. *Opt. Express* **12,** 3428–3435 (2004).
10. Helseth, L. E., Wen, H. Z. & Fischer, T. M. Colloidal optomagnetic dimmer. *Langmuir* **22,** 3941–3944 (2006).
11. Domachuk, P. *et al.* Application of optical trapping to beam manipulation in optofluidics. *Opt. Express* **13,** 7265–7275 (2005).
12. Wu, M. H. & Whitesides, G. M. Fabrication of arrays of two-dimensional micropatterns using microspheres as lenses for projection photolithography. *Appl. Phys. Lett.* **78,** 2273–2275 (2001).
13. Denk, R., Piglmayer, K. & Bäuerle, D. Laser-induced etching and deposition of W using a-SiO_2 microspheres. *Appl. Phys. A: Mater.* **76,** 549–550 (2003).
14. McLeod, E. & Arnold, C. B. Subwavelength direct-write nanopatterning using optically trapped microspheres. *Nature Nanotech.* **3,** 413–417 (2008).
15. Tatarkova, S. A., Carruthers, A. E. & Dholakia, K. One-dimensional optically bound arrays of microscopic particles. *Phys. Rev. Lett.* **89,** 283901 (2002).
16. Wenger, J., Gerard, D., Aouani, H. & Rigneault, H. Disposable microscope objective lenses for fluorescence correlation spectroscopy using latex microspheres. *Anal. Chem.* **80,** 6800–6804 (2008).
17. Kneipp, J. *et al.* Gold nanolenses generated by laser ablation-efficient enhancing structure for surface enhanced Raman scattering analytics and sensing. *Anal. Chem.* **80,** 4247–4251 (2008).
18. Barnes, M. D., Ng, K. C., Whitten, W. B. & Ramsey, J. M. Detection of single Rhodamine 6G molecules in levitated microdroplets. *Anal. Chem.* **65,** 2360–2365 (1993).
19. Brooks Shera, E., Seitzinger, N. K., Davis, L. M., Keller, R. A. & Soper, S. A. Detection of single fluorescent molecules. *Chem. Phys. Lett.* **174,** 553–557 (1990).
20. Furuike, S. *et al.* Temperature dependence of the rotation and hydrolysis activities of F1-ATPase. *Biophys. J.* **95,** 761–770 (2008).
21. Farjadpour, A. *et al.* Improving accuracy by subpixel smoothing in the finite-difference time-domain. *Opt. Lett.* **31,** 2972–2974 (2006).
22. Whitmore, P. M., Alivisatos, A. P. & Harris, C. B. Distance dependence of electronic energy transfer to semiconductor surfaces: $^3n\pi^*$ pyrazine/GaAs(110). *Phys. Rev. Lett.* **50,** 1092–1094 (1983).
23. Sluch, M. I., Vitukhnovsky, A. G. & Petty, M. C. Anomalous distance dependence of fluorescence lifetime quenched by a semiconductor. *Phys. Lett. A* **200,** 61–64 (1995).
24. Campion, A., Gallo, A. R., Harris, C. B., Robota, H. J. & Whitmore, P. M. Electronic energy transfer to metal surfaces: a test of classical image dipole theory at short distances. *Chem. Phys. Lett.* **73,** 447–450 (1980).
25. Crackel, R. L. & Struve, W. S. Non-radiative excitation decay of cresyl violet on TiO_2: variation with dye–surface separation. *Chem. Phys. Lett.* **120,** 473–476 (1985).
26. Farahani, J. N., Pohl, D. W., Eisler, H. J. & Hecht, B. Single quantum dot coupled to a scanning optical antenna: a tunable superemitter. *Phys. Rev. Lett.* **95,** 017402 (2005).
27. Jin, S. & Lian, T. Electron transfer dynamics from single CdSe/ZnS quantum dots to TiO_2 nanoparticles. *Nano Lett.* **9,** 2448–2454 (2009).
28. Robel, I., Kuno, M. & Kamat, P. V. Size-dependent electron injection from Excited CdSe quantum dots into TiO_2 nanoparticles. *J. Am. Chem. Soc.* **129,** 4136–4137 (2007).
29. Chen, C., Qi, X. & Zhou, B. Photosensitization of colloidal TiO_2 with a cyanine dye. *J. Photochem. Photobiol. A* **109,** 155–158 (1997).
30. Schwartz, J. J. & Quake, S. R. Single molecule measurement of the 'speed limit' of DNA polymerase. *Proc. Natl Acad. Sci. USA* **106,** 20294–20299 (2009).
31. Schwartz, J. J. & Quake, S. R. High density single molecule surface patterning with colloidal epitaxy. *Appl. Phys. Lett.* **91,** 083902 (2007).

Acknowledgements

The authors thank M. Brongersma, H.J. Lee and M.F. Yanik for discussions, and E. Townsend for writing the instrumentation software. This work was supported in part by the Department of Defense Advanced Research Projects Agency Optofluidics Center, the National Human Genome Research Institute (5R01HG003594-04), and the Howard Hughes Medical Institute. S.S. was funded by a Marie Curie fellowship (MOIF-CT-2006-0400320 FRETANDFORCE).

Author contributions

J.J.S., S.S. and S.R.Q. conceived and designed the experiments. J.J.S. and S.S. performed the experiments. J.J.S. and S.S. analysed the data. J.J.S., S.S. and S.R.Q. wrote the paper.

Additional information

The authors declare competing financial interests: details accompany the paper at www.nature.com/naturenanotechnology. Supplementary information accompanies this paper at www.nature.com/naturenanotechnology. Reprints and permission information is available online at http://npg.nature.com/reprintsandpermissions/. Correspondence and requests for materials should be addressed to S.R.Q.